 

PACS numbers: 42.65.Hw; 42.65.Sf; 42.70.Nq
DOI: 10.1070/QE2008v038n04ABEH013745

# Dynamics of photorefractive self-pumped phase-conjugate mirrors with a linear resonator

Mehran Vahdani Mogaddam, K.V. Rudenko, V.V. Shuvalov

***Abstract*. The phase-conjugation dynamics in a self-pumped phase-conjugate mirror (SP PCM) based on a $BaTiO_3$ photorefractive crystal (PRC) with a linear resonator is simulated numerically. It is shown that a phased array of dynamic holograms is formed in such a SP PCM under optimal conditions, and the interference of the waves scattered by this array provides the very high stationary phase-conjugation efficiency (the nonlinear reflection coefficient and overlap integral exceeding 80 % and 95 %, respectively). It is found that the development of instabilities is caused both by the violation of phase relations in this array and the formation of additional dynamic holograms in the PRC in the geometry typical of a SP PCM with a semi-linear resonator and by the self-bending effect typical of PRCs.**

***Keywords***: *phase-conjugate mirror with a linear resonator, photorefractive nonlinearity, phase-conjugation dynamics, stable and unstable generation.*

## 1. Introduction

Wavefront distortions appearing during the propagation of coherent radiation in a medium with inhomogeneities of the refractive index can be compensated by using phase-conjugate mirrors (PCMs) based on photorefractive crystals (PRCs) [1]. Self-pumped PCMs (SP PCMs) can operate at input radiation intensities down to a few mW $cm^{-2}$ [2] and do not require pump sources [3, 4]. For example, in double SP PCMs [5 – 7], two incoherent [8] light waves, either orthogonally polarised [9] or with different carrier frequencies [10], are simultaneously phase-conjugated, while lasing is developed (as upon phase conjugation in SRS and SBS mirrors [11]) due to self-organisation [12, 13]. Because of this, although the nonlinear reflection coefficient $R$ and the overlap integral $H$ in the SP PCM achieve their maximum values $R_{max} = 0.8 - 0.9$ and $H_{max} > 0.9$, respectively, the time required for the formation of a PC wave (i.e. for the appearance of dynamic holograms of the required structure in the PRC) is usually tens of seconds and more (see, for example, [14]). The attempts to reduce the response time of SP PCMs by varying the parameters and geometry of the problem [14], increasing the seed noise level [11, 15], using frequency shifts [16, 17], and external permanent [18, 19] or alternating [20 – 22] electrostatic fields lead either to a decrease in the SP PCM efficiency ($R$ and $H$) or to the development of instabilities [2].

It was shown in [23] that in a double SP PCM based on a $BaTiO_3$ PRC, along with a dynamic hologram formed in the self-intersection region of input beams, the additional refractive-index gratings are also produced whose geometry is typical of two-crystal SP PCMs [1]. A competition between these two PC channels leads to a complicated spatiotemporal dynamics of generated fields. The efficient generation of two PC waves ($R_{max} = 0.50 - 0.70$ and $H_{max} = 0.60 - 0.70$) or of something like the dynamic chaos in a system of thin soliton-like filaments becomes possible. It was shown in [24] that for a loop SP PCM based on the same PRC, $R_{max} = 0.80 - 0.90$ for $H_{max} = 0.90 - 0.95$, and the passage to chaos occurs according to a different scenario. In this case, the generation of a PC wave is caused by scattering on a grating formed in the self-intersection region of the forward and backward beams, while the appearance of other types of dynamic holograms leads to instability.

By using calculation methods described in detail in [23, 24] and the same parameters of the problem ($BaTiO_3$ PRC), we show below that in the case of stable generation of a PC wave in a SP PCM with a linear resonator, a set (phased array) of dynamic holograms is formed in the PRC. The interference of the waves scattered by them provides the high PC efficiency ($R_{max} > 0.80$ for $H_{max} > 0.95$). The passage to unstable generation regimes in this case can be caused by the violation of phase relations in this set and the formation of additional dynamic holograms in the PRC in the geometry typical of SP PCMs with a semi-linear resonator [1], as well as by self-action effects.

## 2. Model and scheme of numerical calculations

Figure 1 illustrates the geometry of the model problem under study. As in [23, 24], we assumed that forward and backward light waves with amplitudes $A_{f,b}$ and wave vectors $\boldsymbol{k}_{f,b} = \{k_x, \pm k_z\}$ propagated at small angles ($k_z \gg k_x$) with respect to the positive and negative directions of the $z$ axis from the two opposite faces of the PRC (planes $z = 0$ and $z = L$). Here, $k_{x,z}$ are the projections of the wave vector $\boldsymbol{k}$ on the $x$ and $z$ axes. We

**Mehran Vahdani Mogaddam, K.V. Rudenko, V.V. Shuvalov** International Laser Center, M.V. Lomonosov Moscow State University, Vorob'evy gory, 119992 Moscow, Russia; e-mail: vsh@vsh.phys.msu.su

Received 18 October 2007; revision received 3 December 2007
*Kvantovaya Elektronika* **38** (4) 377 – 382 (2008)
Translated by M.N. Sapozhnikov

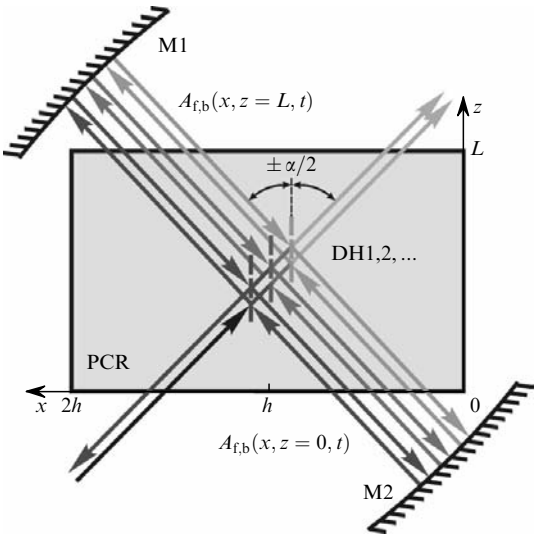


**Figure 1.** Geometry of the interaction of $A_{f,b}(x, z, t)$ waves in a SP PCM with a linear resonator: (PCR) photorefractive crystal; (M1, M2) highly reflecting resonator mirrors; (DH1, 2, ...) dynamic holograms for the first, second, etc. generation channels.

assumed that the backward wave $A_b$ was generated due to reflection of the forward wave $A_f$ from mirror M1 of a linear resonator formed by highly reflecting spherical mirrors M1 and M2 with equal radii of curvature ($R_1 = R_2$). It was assumed that mirrors M1 and M2 were placed directly behind the front and rear faces of the PRC so that the resonator axis was turned through angle $-\alpha/2$ with respect to the $z$ axis and passed through the PRC centre [point $\{x = h, z = L/2\}$], where $2h$ and $L$ are the PRC sizes along the $x$ and $z$ axes, respectively]. In addition, broadband super-Gaussian (32th order) spatial filters were mounted in front of each of the mirrors. The Fourier components of radiation incident on these filters at angles within $\pm 7^\circ$ from the resonator axis are completely transmitted, whereas the reflection of radiation components with the wave vectors directed close to the orientation of the wave vector of the input beam is efficiently suppressed (see below).

As in [23, 24], the nonlinear response dynamics of the PRC was calculated based on a system of microscopic equations [25] for the two-dimensional case (the so-called slit beams [26]) taking into account only transmission dynamic holograms [the vector $\boldsymbol{\kappa}$ of the refractive-index gratings $\delta\eta(x, z, t)$ written in the PRC is directed along the $x$ axis] by neglecting the photovoltaic effect [1, 14, 18]. It was assumed that the external electric field $\delta\eta(x, z, t)$ in the PRC was directed along the $x$ axis and its strength was small ($E_0 = 1$ V cm$^{-1}$). The problem to be solved was transferred to the class of self-consistent problems taking into account the relation of intensity distributions $I_{f,b}(x, z, t) = |A_{f,b}(x, z, t)|^2$ with the intracrystal static field $E_{sc}(x, t) \propto \delta\eta(x, z, t)$, which was specified by standard truncated wave equations for the amplitudes $A_{f,b}(x, z, t)$ of interacting waves [1]. The truncated equations were written in the paraxial approximation by neglecting the spatially homogeneous addition to the refractive index $\eta$ of the PRC, which was caused by the external field. The situation was considered in which the total radiation intensity was determined by the sum of intensities of the forward and backward waves, $I(x, z, t) = I_f(x, z, t) + I_b(x, z, t)$, i.e. the case of incoherent or orthogonally polarised (for example, with the help of an additional $\lambda/4$ phase plate mounted in front of each of the mirrors) counterpropagating waves.

The self-consistent problem was solved by calculating numerically the evolution of distributions $A_{f,b}(x, z, t)$ and $\delta\eta(x, z, t)$ in time. All the variables were described over the grid with the number of nodes on the PCR aperture ($2h = 4$ mm) and along the PCR length ($L = 4$ mm) equal to 8192 and 512, respectively. The initial conditions corresponded to the switching on of the SP PCM at the instant $t = 0$. The input field amplitude $A_f(x, z = 0, t)$ was determined as a linear superposition of the input signal amplitude $A_f^{(0)}(x, z = 0, t)$, the amplitude $A_f^{(r)}(x, z = 0, t)$ of the field reflected from mirror M2, and the amplitude $A_{noise}(x, t)$ of the $\delta$-correlated (taking into account steps along $x$ and $t$) noise, whose average intensity $\langle I_{noise}\rangle = \langle |A_{noise}(x, t)|^2\rangle$ was varied in the range $10^{-6} - 10^{-4}$ of the maximum intensity of the input signal beam $I_{max} = 10 - 150$ mW cm$^{-2}$. The backward wave amplitude in the plane $z = L$ was specified by the superposition of the field $A_b^{(r)}(x, z = L, t)$ reflected from mirror M1 and the same noise $A_{noise}(x, t)$. The spatial intensity distribution $|A_f^{(0)}(x, z = 0, t)|^2$ of the input signal beam at a wavelength of 0.514 μm was assumed Gaussian (the beam width was $2\rho_0 = 100$ μm), its wavefront was plane, and the propagation direction made an angle $\alpha/2 = 7^\circ$ with the $z$ axis. Thus, the period of dynamic holograms written in the PRC was specified by the convergence angle $\alpha = 14^\circ$, which was not varied. The problem was solved in the adiabatic approximation by using the method of separation over physical factors and the fast Fourier transform [27, 28]. As in [23, 24], the time step $\Delta t =$ 0.2 s was set much shorter than the evolution time of the PRC state and most of the parameters of the problem were fixed because their values were determined by the PRC type ($BaTiO_3$, see table in [23, 24]).

The energy efficiency of the SP PCM and the phase-conjugation quality of the input signal were estimated from the instant values of the nonlinear reflection coefficient

$$R(t) = \frac{\int_h^{2h} |A_b(x, z = 0, t)|^2 \mathrm{d}x}{\int_h^{2h} |A_f(x, z = 0, t)|^2 \mathrm{d}x} \qquad (1)$$

and the overlap integral

$$H(t) = \frac{\left| \int_h^{2h} A_f(x, z = 0, t) A_b^*(x, z = 0, t) \mathrm{d}x \right|^2}{\int_h^{2h} |A_f(x, z = 0, t)|^2 \mathrm{d}x \int_h^{2h} |A_b(x, z = 0, t)|^2 \mathrm{d}x}. \qquad (2)$$

The product $RH$ characterises the relative fraction of the power of the PC component in the output field (on the output face of the PRC) at the instant $t$. Note that $R(t)$ and $H(t)$ were calculated by transmitting preliminarily the field $A_b(x, z = 0, t)$ generated in the SP PCM through another spatial filter selecting half the input aperture of the PRC [see integration limits in (1) and (2)] corresponding to the position of the maximum intensity of the input signal beam $A_f^{(0)}(x, z = 0, t)$.

## 3. Stationary generation regime

Figures 2a – c show the shades-of-grey maps of stationary intensity distributions $I_f(x,z)$ (Figs 2a, b) and $I_b(x,z)$ (Fig. 2c) formed in the PRC under conditions close to optimal (for $R_{1,2} = 360$ mm, $I_{max} = 27$ mW cm$^{-2}$, and $\langle I_{noise}\rangle / I_{max} = 10^{-4}$) after the end of the transient process (for $t = 800$ s). Hereafter, the darker regions correspond to the lower values of $I_{f,b}$ and the lighter regions – to the higher values of $I_{f,b}$, and the linear (Fig. 2a) and logarithmic (Figs. 2b, c) shades-of-grey scales are used. On the logarithmic scale, the cut-off is performed at ten natural orders of $I_{max}$. The distribution $I_b(x,z)$ on the linear scale is not presented because it is almost identical to the distribution shown in Fig. 2a. Curves (*1*) in Figs 2d and 2e present the intensity distributions $I_f(x, z = L/2)$ and $I_b(x, z = L/2)$ for forward and backward waves at the central cross section (at the middle of the length) of the PRC at the same instant.

It is easy to verify that the spatial distribution of the field formed in the resonator in the stationary regime is quite unusual. This field represents a system of many (under our conditions, 18) thin (of width down to 9 μm) soliton-like parallel filaments (the diffraction length is $L_d \simeq 0.12$ mm, which is much smaller than $L$). The width and intensity of the filament nearest to the front face of the PRC are considerably greater than these of other filaments (Figs 2d, e). Taking into account absorption in the PRC, this means that an array of dynamic holograms DH1, 2, ... formed in the PRC (Fig. 1), which provide the balance of the energy income and outcome in individual filaments due to the transfer of the input signal energy $A_f^{(0)}(x,z,t)$ during diffraction. Moreover, as we will see below, this array (as the field in filaments themselves) is phased.

The scattering of the input beam by the array of dynamic holograms is the Bragg process, and the beam energy almost completely is transferred to the first diffraction order (see Fig. 2a). However, the presence of the zero order in this process becomes noticeable on the logarithmic scale (Fig. 2b). Under optimal conditions, the overlap integral on the input face of the PRC achieves its maximum value $H_{max} > 0.95$ for almost a limiting value of the nonlinear reflection coefficient $R_{max} > 0.80$ (i.e. limited only by

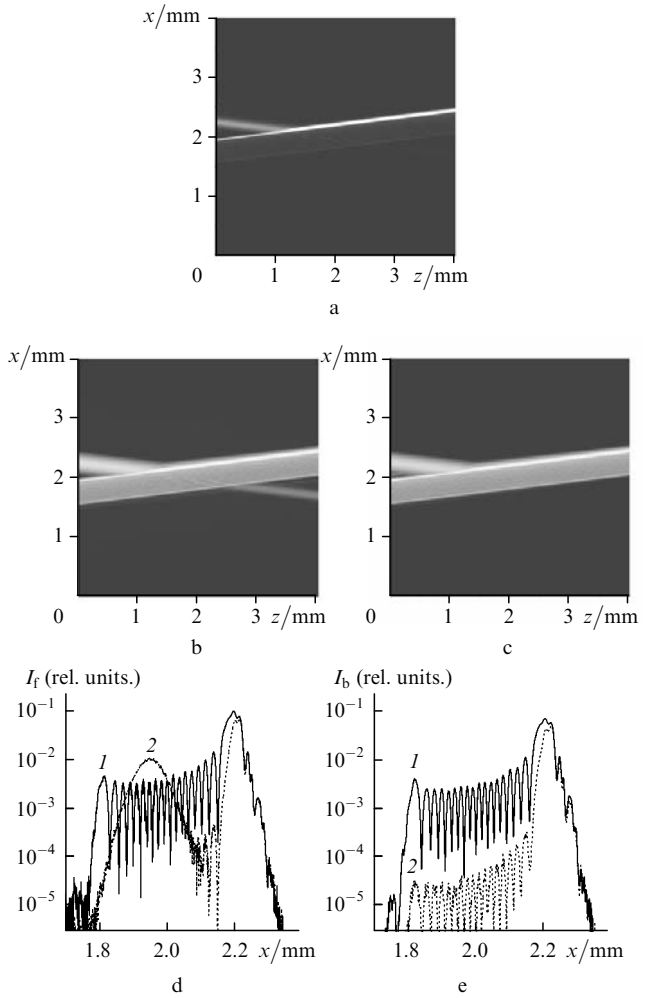


**Figure 2.** Maps of intensity distributions $I_f(x,z)$ (a, b) and $I_b(x,z)$ (c) on the linear (a) and logarithmic (b and c, cut-off at ten natural orders) in $I_{f,b}$ shades-of-grey scales upon stationary phase conjugation of the input Gaussian beam: $R_{1,2} = 360$ mm, $I_{max} = 27$ mW cm$^{-2}$ and $\langle I_{noise}\rangle / I_{max} = 10^{-4}$. Transformation of intensity distributions $I_f(x, L/2)$ (d) and $I_b(x, L/2)$ (e) after instant (at the moment $t = 40$ s) switching off the feedback loop (mirror M2): $I_b(x, L/2)$ before (*1*) and after (*2*) switching-off.

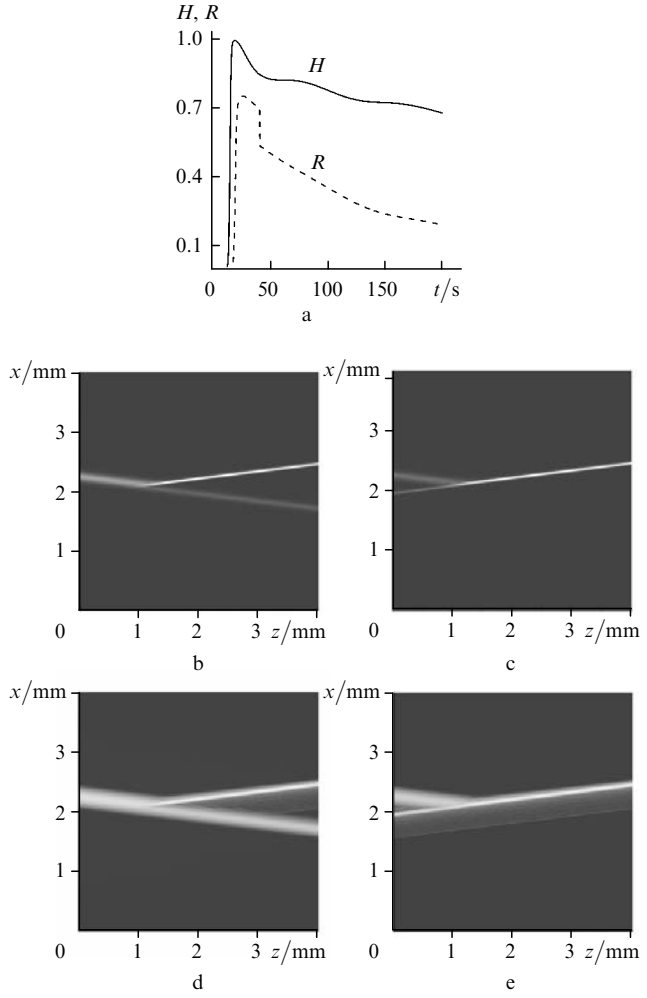


**Figure 3.** Dependences $H(t)$ and $R(t)$ (a) before and after instant (at the moment $t = 40$ s) switching off the feedback loop (mirror M2). Maps of intensity distributions $I_f(x,z)$ (b, d) and $I_b(x,z)$ (c, e) on the linear (b, c) and logarithmic (d, e, cut-off at ten natural orders) in $I_{f,b}$ shades-of-grey scales immediately after switching-off: $R_{1,2} = 360$ mm, $I_{max} = 27$ mW cm$^{-2}$ and $\langle I_{noise}\rangle / I_{max} = 10^{-4}$.

absorption), while the duration of the transient process is about 20 s (Fig. 3a). The phasing of the array of dynamic holograms DH1, 2, ... is proved by the transformation of the intensity distributions $I_f(x,z)$ and $I_b(x,z)$, which occurs at once after the instant (at the moment $t = 40$ s) switching-off of the feedback loop (mirror M2). This transformation is illustrated in Figs 3b–e for the same parameters as in Fig. 2 ($R_{1,2} = 360$ mm, $I_{max} = 27$ mW cm$^{-2}$ and $\langle I_{noise}\rangle/I_{max} = 10^{-4}$). In the case of such switching-off of the resonator, dynamic holograms DH1, 2... cannot change at once due to the delayed response of the PRC and any transformation of distributions $I_{f,b}(x,z)$ in Figs 3b–e with respect to distributions shown in Figs 2a–c can be caused only by changes in the illumination conditions of the PRC. One can see from Fig. 3a that the overlap integral $H$ does not change at once in this case, while the nonlinear reflectance $R$ of the SP PCM changes abruptly, instantly decreasing down to $\sim 0.5$. The intensity distributions $I_f(x,z)$ in the PCR are also instantly transformed. Figure 3b (the linear scale of shades of grey) demonstrates the zero diffraction order, and Fig. 3c (the logarithmic scale) shows that, although the diffraction efficiency of dynamic holograms DH2, ... is comparatively low, the transfer of the input signal energy to soliton-like filaments continues. This is also confirmed by the instant change in the intensity distributions $I_f(x, z = L/2)$ (Fig. 2d) and $I_b(x, z = L/2)$ (Fig. 2e) of the forward and backward waves in the central cross section of the PRC at the moment of the resonator switching-off [the transformation of dependences (*1*) to (*2*)].

It follows unambiguously from the above discussion that almost complete quenching of the zero order of the input signal diffraction by the array of dynamic holograms DH1, 2, ... in the stationary generation regime, which leads to a considerable difference between distributions $I_f(x,z)$ before (Figs 2a, b) and after (Figs 3c, d) instant resonator switching-off, has a purely interference nature and both the array of dynamic holograms and the field in all soliton-like filaments are phased.

## 4. Transient processes and development of instabilities

Figure 4 illustrates the time dependences of the nonlinear reflectance $R(t)$ and the overlap integral $H(t)$ after switching on the SP PCM for the case considered above and some other cases. As in the loop [23] and double [24] SP PCMs, the time during which the phase transition occurs in the SP PCM with a linear resonator (which is manifested in the appearance of the field component conjugated with respect to the input signal) decreases with increasing the relative level of the input noise $\langle I_{noise}\rangle/I_{max}$ (Figs 4a, b). When other parameters of the problem deviated from their optimal values, the stability of phase conjugation drastically decreased. Thus, as the input beam intensity $I_{max}$ was increased [Figs 4c, d, $I_{max} = 55$ and 82 mW cm$^{-2}$, curves (*2*) and (*3*)] and the radii of curvature $R_{1,2}$ of mirrors M1, 2 of the linear resonator are decreased (Fig. 4e, $R_{1,2} = 24$ mm), the generation regime became unstable. While in the first case the most noticeable changes occur depending on $H(t)$ (Fig. 4c), in the second case, the phase-conjugation quality deteriorates and the energy efficiency of the SP PCM decreases (Fig. 4e).

The development of instabilities in the SP PCM at high input-signal intensities ($I_{max} = 55$ mW cm$^{-2}$) is illustrated in

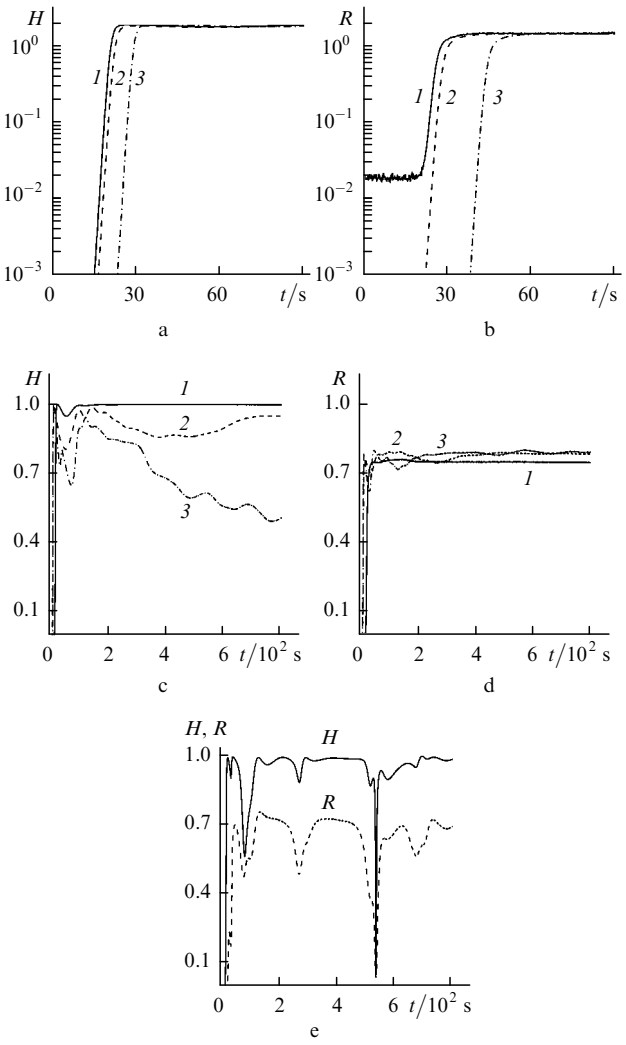


**Figure 4.** Transformation of dependences $H(t)$ (a, c, e) and $R(t)$ (b, d, e) with changing the noise level [a, b; $\langle I_{noise}\rangle/I_{max} = 10^{-4}$ (*1*), $10^{-5}$ (*2*), and $10^{-6}$ (*3*) for $R_{1,2} = 360$ mm and $I_{max} = 27$ mW cm$^{-2}$], the maximum input-beam intensity [c, d; $I_{max} = 27$ (*1*), 55 (*2*), and 82 mW cm$^{-2}$ (*3*) for $R_{1,2} = 360$ mm and $\langle I_{noise}\rangle/I_{max} = 10^{-4}$], and the radii of curvature $R_{1,2}$ of resonator mirrors M1,2 (e; $R_{1,2} = 24$ mm, $I_{max} = 27$ mW cm$^{-2}$, and $\langle I_{noise}\rangle/I_{max} = 10^{-4}$).

Fig. 5, where the maps of intensity distributions $I_b(x,z)$ are presented on the shades-of-grey scale linear in $I_b$ at different instants $t$. First a phased array of similar (due to their low diffraction efficiency) dynamic holograms DH1, 2, ... is formed and a regular system of thin soliton-like filaments of approximately the same intensity oriented parallel to the resonator axis appears (Fig. 5a). Due to the growth of the diffraction efficiency of DH1, the role of this hologram in the generation process increases, and a filament nearest to the front face of the PRC becomes considerably more intense than all the other filaments (Figs 5b, c), Then, additional filaments begin to split from this most intense filament (Fig. 5d). The intersection points of these filaments with the input signal beam are even more displaced to the front face of the PRC and their direction does not coincide with the resonator axis direction. This means that additional dynamic holograms are gradually formed in the PRC in the geometry typical of SP PCMs with a semi-linear resonator [1]. As a result, the additional generation channel appears in the SP PCM, and the geometry of this channel corresponds

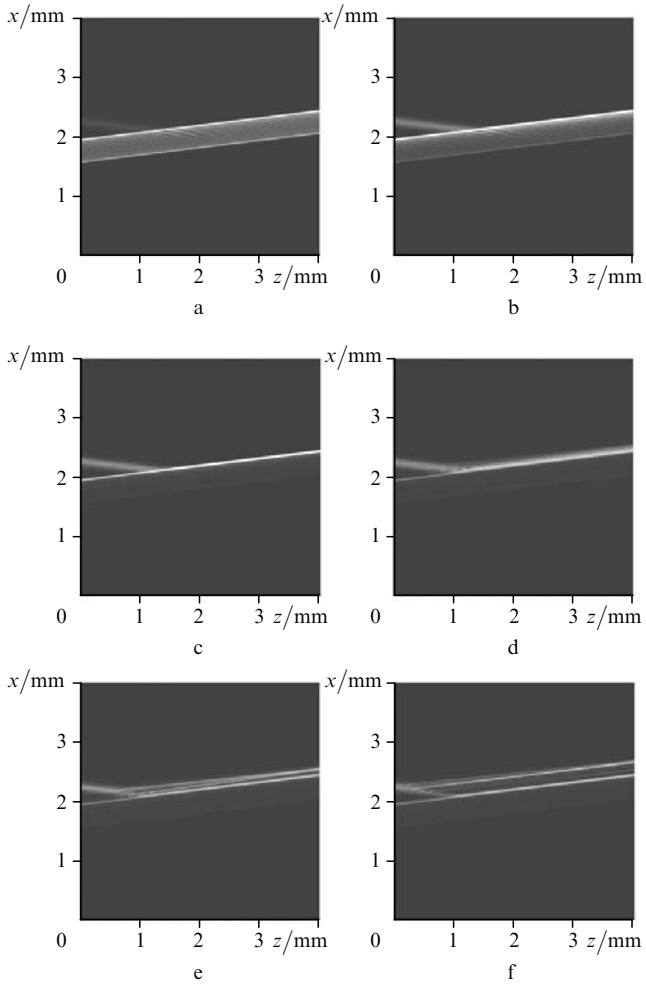


**Figure 5.** Development of the PC wave generation for $R_{1,2} = 360$ mm, $I_{max} = 55$ mW cm$^{-2}$ and $\langle I_{noise}\rangle/I_{max} = 10^{-4}$. Maps of the intensity distribution $I_b(x, z)$ on the shades-of-grey scale linear in $I_b$ are presented at instants $t = 18$ (a), 20 (b), 24 (c), 180 (d), 220 (e) and 500 s (f).

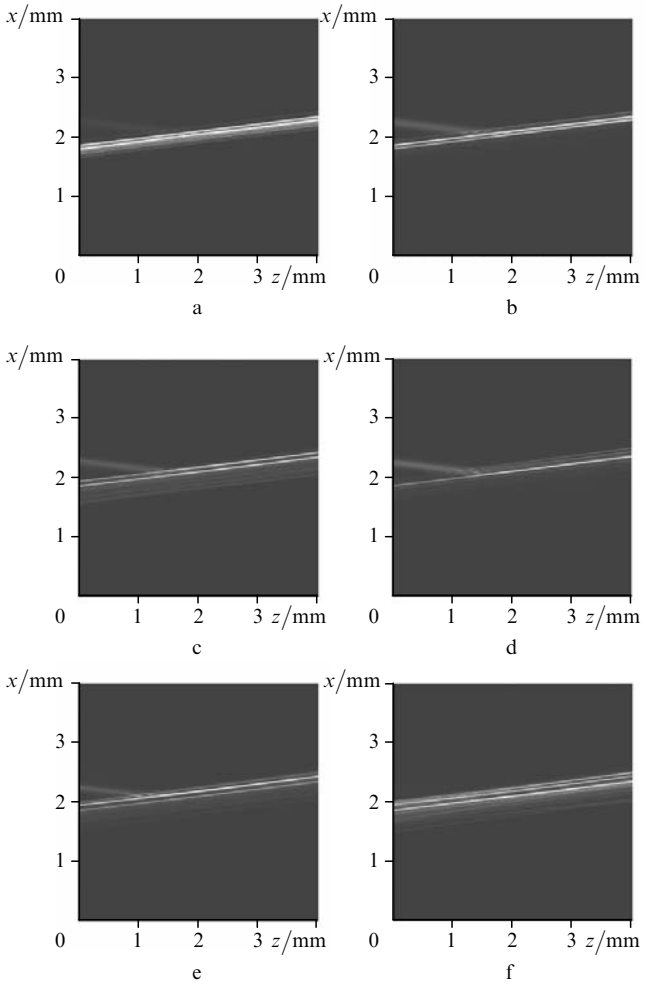


**Figure 6.** Development of the instability for $R_{1,2} = 24$ mm, $I_{max} = 55$ mW cm$^{-2}$ and $\langle I_{noise}\rangle/I_{max} = 10^{-4}$. Maps of the intensity distribution $I_b(x, z)$ on the shades-of-grey scale linear in $I_b$ are presented at instants $t = 36$ (a), 43 (b), 73 (c), 131 (d), 272 (e) and 536 s (f).

to the scheme of a multipass amplifier. The intensity of split-off filaments increases gradually (Fig. 5e) and they cease to reach mirror M2 and reflect from it (Fig. 5f). Thereafter different phase-conjugation channels become independent, the phase relations between PC waves in them are violated and a kind of dynamic chaos appears in the SP PCM and the phase-conjugation quality drastically decreases (Fig. 4c).

The development of instability in the SP PCM in the case of too small radii of curvature $R_{1,2}$ of resonator mirrors M1,2 ($R_{1,2} = 24$ mm) is illustrated in Fig. 6, where the maps of the intensity distribution $I_b(x, z)$ are shown at different instants $t$ on the same shades-of-grey scale. Although in this case, a phased array of similar dynamic holograms DH1, 2, ... and a system of soliton-like filaments of approximately the same intensity are also formed in the PRC, the role of two dynamic holograms is simultaneously distinguished due to the growth of their diffraction efficiency, and two filaments become simultaneously considerably more intense than all the others (Fig. 6a). The position of these filaments differs from the case considered above: they prove to be localised closer to the resonator axis. Moreover, the number of distinguished filaments and their position change during the development of generation (Figs 6a – f), while other filaments become unparallel and begin to intersect (Figs 6c – f) due to the so-called self-bending effect [26], which is typical of PRCs. As a result, different phase-conjugation channels also become independent, and a kind of dynamic chaos appears in the SP PCM. However, changes in the nonlinear reflectance $R(t)$ and the overlap integral $H(t)$ in this case are correlated in time (Fig. 4e), and the SP PCM can cease to reflect any light at certain instants (Figs 4e and 6f).

## 5. Conclusions

We have simulated numerically the phase-conjugation dynamics in the SP PCM (photorefractive $BaTiO_3$ crystal) with a linear resonator and have shown that in the case of stable generation of a PC wave, a set (phased array) of dynamic holograms is formed in the SP PCM, and the interference of the waves scattered by these holograms provides the high phase-conjugation efficiency ($R_{max} > 0.80$ for $H_{max} > 0.95$). In this case, the field with the soliton-like transverse structure is excited in the resonator and the scenario of going to unstable generation regimes principally differs from scenarios for the loop [23] and single-crystal double [24] SP PCM. The development of instabilities in the SP PCM with a linear resonator is caused by the violation

of phase relations in this set and formation of additional dynamic holograms in the geometry typical of SP PCMs with a semi-linear resonator [1], as well as by self-bending effects [26].

The results obtained in the paper are in good qualitative agreement with experimental data. However, the quantitative comparison cannot be performed. This is explained by the fact that PRCs contain many defects in principle and, therefore, characteristics of crystals of even the same type can differ more than by an order of magnitude. In most cases, all the parameters of PRCs required for simulations are not measured and the interpretation of experimental data in terms of a multiparametric model becomes too complicated. At the same time, taking into account that numerical simulations were performed in this paper and in [23, 24] within the framework of the identical model (including the same values of all numerical parameters), the principal difference between data obtained for SP PCM with different types of resonators can be explained only by the difference in the methods of realisation of the feedback loop.

***Acknowledgements.*** This work was supported by the Russian Foundation for Basic Research (Grant No. 06-02-1604).

## References

1. Odulov S.G., Soskin M.S., Khizhnyak A.I. *Lazery na dinamicheskikh reshetkakh: opticheskie generatory na shetyrekhvolnovom cmeshchenii* (Dynamic Grating Lasers: For-Wave-Mixing Optical Oscillators) (Moscow: Nauka, 1990).
2. Mailhan C., Fressengeas N., Goetz M., Kugel G. *Phys. Rev. A*, **67** (2), 023817 (2003).
3. Feinberg J. *Opt. Lett.*, **7** (10), 486 (1982).
4. Cronin-Golomb M., Fischer B., White J.O., Yariv A. *Appl. Phys. Lett.*, **41** (8), 689 (1982).
5. Kwong S.-K., Cronin-Golomb M., Yariv A. *IEEE J. Quantum Electron.*, **22** (8), 1508 (1986).
6. Weiss S., Sternklar S., Fischer B. *Opt. Lett.*, **12** (2), 114 (1987).
7. Fischer B., Sternklar S., Weiss S. *IEEE. J. Quantum Electron.*, **25** (3), 550 (1989).
8. Segev M., Weiss S., Fischer B. *Appl. Phys. Lett.*, **50** (20), 1397 (1987).
9. Kung H.C., Yau H.F., Lee H.Y., Kukhtarev N., Chen T.C., Sun C.C., Chang C.C., Tong Y.P. *Opt. Lett.*, **25** (14), 1031 (2000).
10. Sternklar S., Fischer B. *Opt. Lett.*, **12** (9), 711 (1987).
11. Zel'dovich B.Ya., Pilipetskii N.F., Shkunov V.V. *Obrashchenie volnovogo fronta* (Phase Conjugation) (Moscow: Nauka, 1985).
12. Engin D., Orlov S., Segev M., Valley G.C., Yariv A. *Phys. Rev. Lett.*, **74** (10), 1743 (1995).
13. Odoulov S.G., Goulkov M.Yu., Shinkarenko O.A. *Phys. Rev. Lett.*, **83** (18), 3637 (1999).
14. Gunter P., Huignard J.-P. (Eds) *Photorefractive Materials and Applications. Topics in Applied Physics* (Heidelberg: Springer, 1988 – 1989) Vols 61 – 62.
15. Krause A., Notni G., Wenke L. *Opt. Mater.*, **4** (2), 386 (1995).
16. MacDonald K.R., Feinberg J. *Phys. Rev. Lett.*, **55** (8), 821 (1985).
17. Zel'dovich B.Ya., Kundikova N.D., Naumova I.I. *Kvantovaya Elektron.*, **19**, 785 (1992) [*Quantum Electron.*, **22**, 725 (1992)].
18. Petrov M.P., Stepanov S.I., Khomenko A.V. *Fotorefraktivnye kristally v kogerentnoi optike* (Photorefractive Crystals in Coherence Optics) (St. Petersburg, Nauka, 1992).
19. Kamshilin A.A., Nazhestkina N., Kobozev O.V., Jaaskelainen T. *Opt. Lett.*, **26** (8), 527 (2001).
20. Zel'dovich B.Ya., Nesterkin O.P., Novikov A.V., Shershakov E.P. *Pis'ma Zh. Eksp. Teor. Fiz.*, **56**, 301 (1992).
21. Esselbach M., Cedilnik G., Kiessling A., Baade T., Kowarschik R., Prokofiev V. *J. Opt. A: Pure Appl. Opt.*, **1** (6), 735 (1999).
22. Taj I.A., Xie P., Mishima T. *Opt. Commun.*, **187** (1-3), 7 (2001).
23. Mogaddam M. Vahdani, Shuvalov V.V. *Kvantovaya Elektron.*, **35**, 658 (2005) [*Quantum Electron.*, **35**, 658 (2005)].
24. Mogaddam M. Vahdani, Shuvalov V.V. *Kvantovaya Elektron.*, **35**, 862 (2005) [*Quantum Electron.*, **35**, 862 (2005)].
25. Kukhtarev N.V., Markov V.B., Odulov S.G., Soskin M.S., Vinetskii V.L. *Ferroelectrics*, **22** (3), 949 (1979).
26. Duree G., Salamo G., Segev M., Yariv A., Crosignani B., DiPorto P., Sharp E. *Opt. Lett.*, **19** (16), 1195 (1994).
27. Vysloukh V.A., Kutuzov V., Shuvalov V.V. *Kvantovaya Elektron.*, **23**, 157 (1996) [*Quantum Electron.*, **26**, 153 (1996)].
28. Vysloukh V.A., Kutuzov V., Shuvalov V.V. *Kvantovaya Elektron.*, **23**, 881 (1996) [*Quantum Electron.*, **26**, 858 (1996)].